Pergamon

Int. J. Heat Mass Transfer. Vol. 40, No. 8, pp. 1885–1894, 1997

0017–9310/97 $17.00+0.00

PII: S0017–9310(96)00225–6

Forced convection in an air-filled bayonet tube during the laminar–turbulent transition

HARPAL MINHAS and G. S. H. LOCK

Department of Mechanical Engineering, University of Alberta, Edmonton, Alberta, Canada T6G 2G8

(*Received* 27 *February* 1996 *and in final form* 10 *June* 1996)

Abstract—The paper provides details of a numerical study of the bayonet tube during the laminar–turbulent transition when the fluid is air. Attention is focused on the heat transfer characteristics of the tube. The data constitute a systematic investigation of the effect of several parameters on the overall heat transfer rate, represented by a Nusselt number. Specifically discussed are the effects of inner tube conductance, Reynolds number, and length-diameter ratio. Results are interpreted in terms of the origin and spread of turbulence, as revealed by the turbulence intensity contours calculated from the k–ε model. Comparisons are made with available experimental data.

1. INTRODUCTION

The bayonet tube is a refluent heat exchanger. As shown in Fig. 1, it is constructed from two concentric tubes with one end of the inner tube (diameter d) reaching to within a distance H from the sealed end of the outer tube (diameter D). Fluid flowing first inside the inner tube is thus constrained to return along the annular gap formed between the two tubes. The system is commonly used under conditions where the medium to be heated or cooled is either too large to be treated in its entirety or is readily accessible from one side only. A more extensive discussion is given by Lock [1].

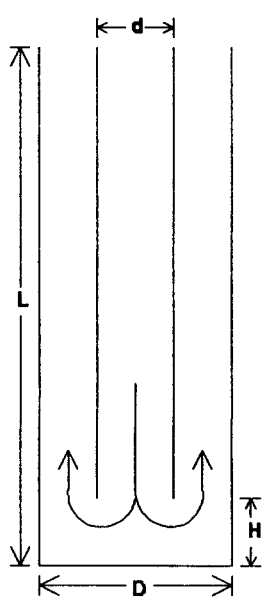

Fig. 1. Dimensions of the bayonet tube.

In geotechnical applications, bayonet tubes may be used to penetrate the earth's surface. In regions containing sporadic permafrost, for example, the internal circulation of a refrigerant, or cold winter air, serves to maintain the ground in a frozen state in which it can support engineering structures such as towers, buildings or roads [2, 3]. Similarly, bayonet tubes inserted through the winter ice cover on a river may be used to create a submerged wall of ice to facilitate the control of spring run off [4].

Bayonet tubes are also used in the process industries. Some of the earlier applications are found in vacuum condensers, suction tank heaters and alkylation contactors [5]. Recently, they have been used in a variety of applications: a potassium condenser boiler in a binary cycle power plant [6], a counterflow heat exchanger in a chemical processing plant [7], a water tube reformed gas boiler in an ammonia plant [8] and a high temperature burner duct recuperator in a steel mill soaking pit [9].

The device was first studied systematically in the experimental work of Idel'Chik and Ginzburg [10]. They discovered a strong influence of clearance ratio. A numerical study by Yang and Hsieh [11] detected a vortex in the end clearance zone. Laboratory tests by Lock and Wu [12] and a numerical study by Minhas [13] confirmed the presence of the end vortex. Later, Lock and Wu [14] studied the effects of mass flow rate and tube geometry on the thermal performance of the tube.

Although a typical industrial application of the bayonet tube requires turbulent flow conditions, the effect of a pump or blower failure can only be estimated at much lower Reynolds numbers. Also, several geotechnical and biomedical applications occur in the laminar or transitional range.

This paper extends the earlier work of Lock and

NOMENCLATURE

c	back conduction
d	inner tube diameter
D	outer tube diameter
Eu	Euler number
F	flow area
h	specific enthalpy
H	end clearance; total enthalpy
i	turbulence intensity
k	turbulence kinetic energy
L	overall length of bayonet tube
m	mass
Nu	Nusselt number
P, p	pressure
q	local heat flux
Q	total heat flux
r	radial distance
Re	Reynolds number
T	temperature
u	turbulent velocity
U	velocity
W	thickness of inner tube
x	axial distance.

Greek symbols

ε	rate of dissipation of turbulent kinetic energy
λ	thermal conductivity
μ	fluid dynamic viscosity
ν	momentum diffusivity
ϕ	normalized temperature
ρ	mass density.

Subscripts

a	annulus
b	bulk
cond	conductor
d	inner tube
f	fluid mean
i	inlet
ins	insulator
w	outer tube wall.

Superscripts

·	per unit time
c	characteristic.

Wu [12, 14] and Minhas [13] covering heat and fluid flow characteristics under laminar conditions. Particular attention is focused on the laminar–turbulent transition. A numerical analysis is used to explore the origin and spread of turbulence and its effect on heat transfer. The study has been conducted over a wide range of selected governing parameters: conductivity ratio, Reynolds number and length–diameter ratio. The area ratio was fixed at 0.474, and the clearance ratio at 1.0; these correspond to a minimum pressure drop and therefore represent an 'optimal' in the hydraulic design under laminar conditions [12]. Comparisons are made with earlier experimental data.

2. NUMERICAL FORMULATION

2.1. *Governing equations and boundary conditions*

Forced convection in a bayonet tube is governed by the continuity and energy equations together with the momentum equation. Neglecting buoyancy, the governing equations for steady, turbulent flow of a Newtonian, Boussinesquian fluid may be written as:

Continuity,

$$\nabla \cdot \rho U = 0. \tag{1}$$

Momentum,

$$\nabla \cdot (\rho U \times U) = \nabla \cdot (\sigma - \overline{\rho u \times u}) \tag{2}$$

where

$$\sigma = -p\delta + \mu(\nabla U + (\nabla U)^T). \tag{3}$$

Energy,

$$\nabla \cdot (\rho U H + \overline{\rho u h} - \lambda \nabla T) = 0 \tag{4}$$

where

$$H = h + \tfrac{1}{2}U^2 + k. \tag{5}$$

The above equations were written in cylindrical coordinates assuming axi-symmetry. All properties, except the fluid density, were taken as constant, magnitudes being evaluated at the average temperature between the inlet T_0 and the outer tube wall T_w. Radiation has not been included because a preliminary calculation for the situation under consideration indicates that radiative heat exchange is very much less than 1% of the total.

Boundary conditions were handled as follows. A long, insulated extension tube ($L/D \approx 200$) attached to the upper end of the bayonet tube was used to create representative conditions at inlet and outlet. An isothermal and hydrodynamically fully developed condition was thus imposed at the entrance to the inner tube while a Neumann condition (zero axial gradients) was established at the extension tube outlet. The k and ε values at the extension tube inlet were taken to be $0.002U_i^2$ and $(0.002U_i)^{1.5}/0.3d_i$, respectively, U_i being the inlet fluid velocity and d_i the inside diameter of inner tube. A characteristically thin inner tube ($W/D = 0.041$) was incorporated. The velocity

at all walls was taken to be zero. The bottom of the outer tube was taken to be insulated. Temperatures were taken to be the same as in the experiments of Lock and Wu [14] thus permitting comparison. Data have been obtained with the inner tube as a perfect insulator ($\lambda_i = 0$) and a perfect conductor ($\lambda_i = \infty$). Symmetry was assumed at the tube centre and periodicity at the plane $\theta = 0, 2\pi$.

2.2. *Definitions*

The results given below are expressed in terms of the following parameters, divided into three categories.

A. Geometry. (1) Length–diameter ratio: L/D, where L and D are the length and diameter, respectively, of the outer tube.

(2) Area ratio: F_i/F_a, where F_i and F_a are the inner tube and annulus areas, respectively. This was held constant.

(3) Clearance ratio: H/D, where H is the end clearance of the inner tube; also fixed.

(4) Inner tube thickness ratio: W/D, where $W = (d_0 - d_i)/2$ is the inner tube thickness; also fixed.

B. Flow rate. Reynolds number. Following Lock and Wu [12], the Reynolds number was defined by

$$Re = \frac{4\dot{m}D}{\rho\pi\nu(D+d_0)d_i} \tag{6}$$

where d_0, d_i are the outside and inside diameters of the inner tube, respectively. This was chosen to accommodate the limiting cases of $d_i \ll D$ and $D \approx d_i$, given the assumption that $d_0 - d_i \ll D$, i.e. $W/D \ll 1$.

C. Conductance. Conductivity ratio. λ_f/λ_i, where λ_f and λ_i are the fluid and inner tube thermal conductivities, respectively. The above parameters, treated as independent variables, may be expected to influence the overall system performance, as measured by the following parameters, treated as dependent variables.

1. *Euler number.* Again following Lock and Wu [12], the Euler number Eu was taken as:

$$Eu = \frac{2\Delta P}{\rho(U^c)^2} \tag{7}$$

where

$$\Delta P = \Delta P_t + \rho U_i^2 \left[1 - \frac{3}{4}\left(\frac{F_i}{F_a}\right)^2\right] \tag{8}$$

and the characteristic velocity scale U^c is given by

$$U^c = \frac{4\dot{m}D^2}{\rho\pi(D^2 - d_0^2)d_i^2}. \tag{9}$$

2. *Nusselt number.* The average Nusselt number was defined in terms of the mean fluid temperature difference in the annulus, i.e. $T_w - T_f$. The Nusselt number, Nu, is thus given by:

$$Nu = \frac{\dot{Q}(D-d_0)}{\pi\lambda_f DL(T_w - T_f)} \tag{10}$$

where

$$T_f = \frac{T_0 + T_b}{2} \tag{11}$$

T_0 and T_b being the fluid bulk temperatures at the inlet and outlet, respectively.

2.3. *Algorithm and program validation*

The numerical simulation was done using version 3.2.1. of Flow3d package of Harwell Laboratory in the U.K. The differential equations were discretized using the SIMPLE-C algorithm [15]. While there is no perfect turbulence model for the laminar–turbulent transition in a bayonet tube, the k–ε model appears to be well adapted to recirculating flow. The Jones and Launder [16] modification makes it suitable for nearly parallel flows in long tubes. This assumption is borne out by our experimental data. The model has the advantage that it does not require a laminar-turbulent switch [17]. It has been successfully applied to relaminarizing flows [18] which also occurs in our situation.

The computational domain was divided into 11 blocks (see Fig. 2). A 20×20 grid was used for blocks 1, 2, 3, 4, 8, 9, 10 and 11. It was anticipated that a finer grid would be needed to accommodate a more complex field in the end clearance space. A 40×20 grid for blocks 5 and 7, and a 40×4 grid for block 6 were therefore used. A convergence factor of 0.65 was employed. A monitoring point was chosen at the center of the upper face of block 9. The convergence criterion required agreement of successive averaged values of the dependent primitive variables at this point to be within 1%. Convergence also required the sum of the absolute values of net mass fluxes into or out of every cell in the flow to be less than 10^{-4} kg s^{-1}.

The program was first run at 'standard' parametric values: $Re = 875$, $L/D = 20$, $F_i/F_a = 0.474$, $H/D = 1$ and $W/D = 0.041$ represent practical operational values for a bayonet tube [12]; this same study also indicated, $F_i/F_a \approx 0.474$ $H/D \approx 1.0$ correspond to an 'optimal' in the hydraulic design. As will be discussed later, the above Reynolds number represents the onset of the laminar-turbulent transition. An accuracy test with the grid size halved, indicated Euler number and Nusselt number changes of less than 3%, while this increased the time taken to run the program by more than 10 times. The program run in three dimensions generated a Nusselt number change of less than 3%. Results were spot checked for uniqueness by using different initial fields ($Re = 0$, 400 and 600). The solutions remained unchanged.

3. DISCUSSION OF RESULTS

The local heat flux, q ($= \partial T/\partial r$) is plotted as a function of distance $X' = (L - X)/D$, where X' is the non-dimensional axial distance from the closed end, and L is the outer tube length, in Fig. 3. This reflects the reconciliation of the refluent flow in the clearance

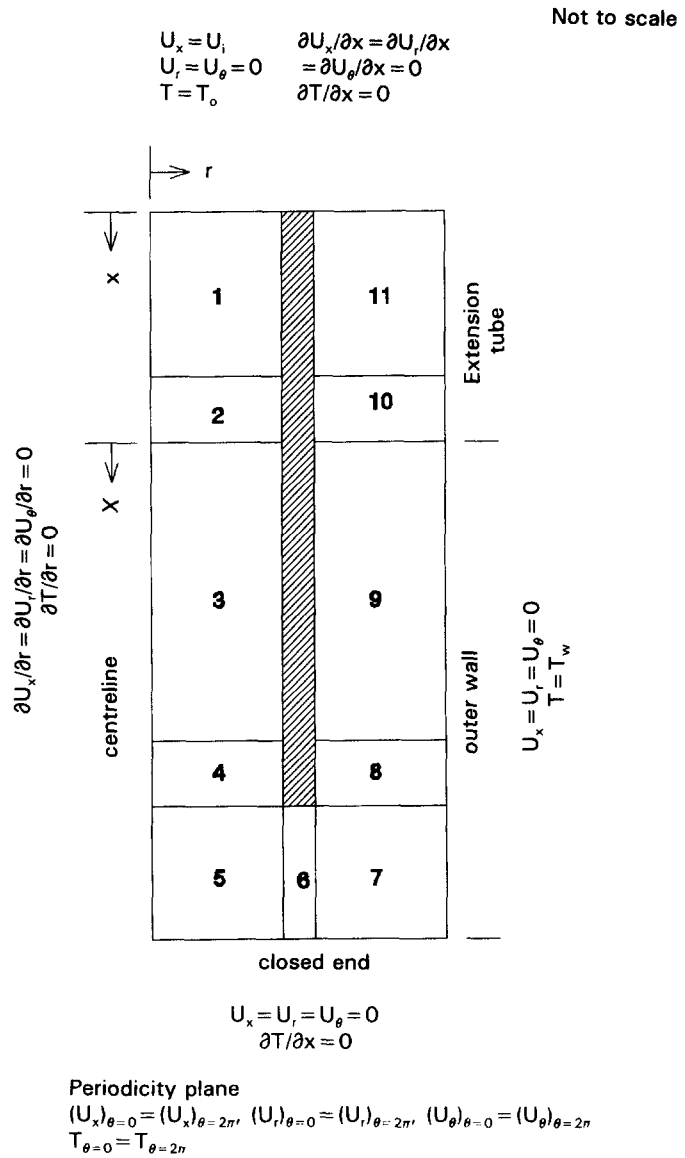

Fig. 2. The computational domain.

zone ($X' < 1.0$) and the developed flow in the annulus ($X' \gg 1.0$). Apart from the slight reduction in heat transfer in the stagnant corner, e.g. $X' < 0.1$, the general shape is formed by the merging of two curves: $X' \leqslant 0.4$, in the presence of a vigorous recirculation; and $X' \geqslant 1.0$, where an entry flow exists. As shown, the details of the reconciliation include a local minimum, corresponding to a local stagnation point on the wall, and a local maximum, following a brief and weak acceleration. The shape of the curve is similar to that obtained under laminar conditions [19].

3.1. *Fluid flow*

The frictional behaviour of the bayonet tube at low mass flow rates (1.27×10^{-4} kg s^{-1} $< \dot{m} < 9.502 \times 10^{-4}$ kg s^{-1}) was studied first, assuming the tube surfaces to be smooth. The numerical results plotted in Fig. 4 are compared with the available experimental data [12] and the results of a previous numerical study [13] under laminar conditions. Agreement with experimental and previous numerical data below $Re = 875$ is within allowable error: $\pm 10\%$ and $\pm 3\%$ for the former and latter, respectively. For numerical data above $Re = 875$, the deviations are larger because the flow is no longer laminar. It is interesting to note that for $Re < 875$ the curve slope is -0.88 as compared to -1.0 in the Moody diagram.

For the tube geometry examined here ($L/D = 20.75$, $F_i/F_a = 0.474$, $H/D = 1.0$), the inner tube and annulus Reynolds numbers are $Re_d = 1.62$ Re and $Re_a = 0.56$ Re, respectively. Inside the inner tube, the transition might be expected to start at $Re \approx 1480$ corresponding to $Re_d = 2400$. However, the discontinuity in the Re–Eu curve in Fig. 4 suggests transition begins earlier at $Re \approx 875$. The onset evidently occurs in the high shear field in the clearance

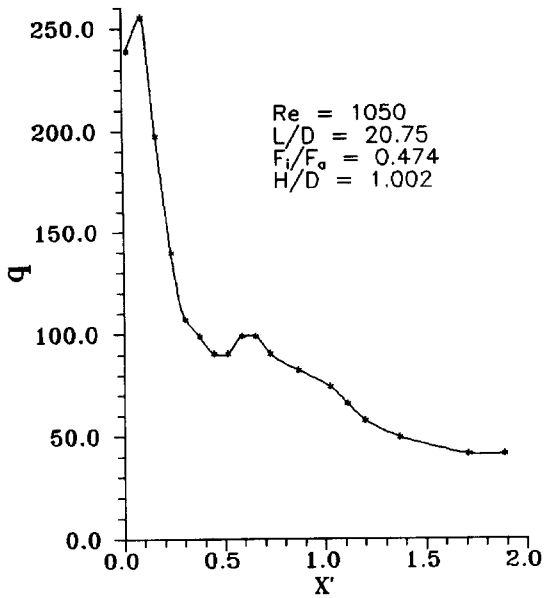

Fig. 3. Heat flux distribution on the outer tube.

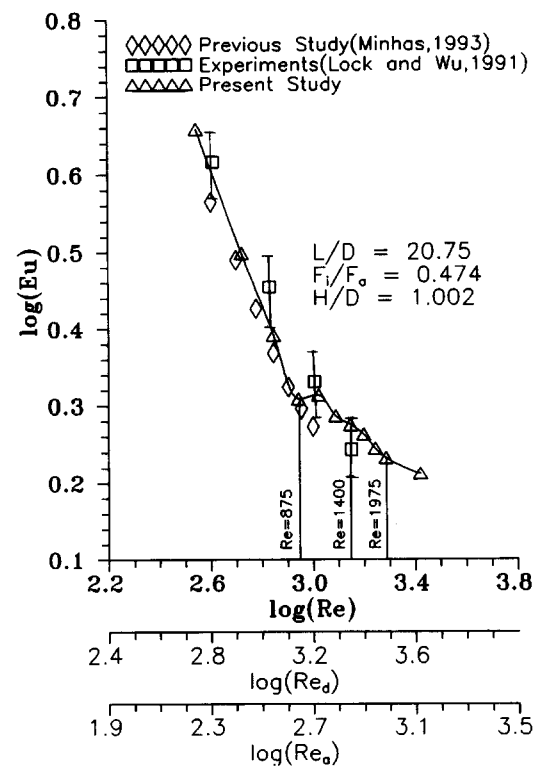

Fig. 4. Frictional characteristics of a smooth bayonet tube.

zone where random disturbances are not easily damped by an adjacent wall. Figure 5 provides an examination of the contours of turbulence intensity $i = (2k/3)^{0.5}/\bar{u}$, where $\bar{u}$ is the inlet velocity at $Re = 1400$. In the clearance zone, very low values of i at $Re = 875$ were found, implying that the flow is laminar for all practical purposes. Figure 5(a) shows how rapidly the intensity increases between $Re = 875$ and 960.

When Re reaches 875, a sudden change is noted on the curve in Fig. 4. With a further increase in Reynolds number the turbulence first spreads through the clearance zone before entering the annulus (Fig. 5(b)). The critical Reynolds number for the inner tube is reached at about $Re = 1400$ i.e. $Re_d = 2270$. The narrow space in the annulus tends to damp the turbulent fluctuations thereby producing a gradual return to laminar conditions. The range $875 < Re < 1240$ is evidently a regime of rapid transition where as $1240 < Re < 1975$ is perhaps best described as an extended transitional range in which the downstream region of the annulus is gradually occupied by the turbulence field as the Reynolds number increases. The flow is fully turbulent everywhere for $Re > 1975$; that is, with $i > 0.1\%$ at the exit. The results presented here refer principally to the range $875 < Re < 1975$ identified as the laminar–turbulent transition range.

3.2. *Heat flow*

3.2.1. *Effect of Reynolds number.* Figures 6 and 7 show the effect of Reynolds number on the thermal regime for different values of the length–diameter ratio when the inner tube is a perfect conductor. As expected, Nu increases with an increase in Re. Figure 6 indicates that the effect is slightly greater under laminar conditions with a shallow slope discontinuity being evident at the onset of transition.

Figure 7(a)–(d) shows the isotherms for $Re = 350$, 875, 1050 and 1225, respectively. Since the bottom of the tube is insulated, the isotherms near the bottom corner tend to be closer together reflecting the ability of the inner tube to carry cool fluid towards the heated wall. Previous work [20] revealed a ring vortex dominating flow in the clearance zone. For $Re \approx 875$, turbulent mixing begins to influence the isotherm pattern dramatically. Thereafter, the clearance vortex approximates an isothermal (cool) region while radial temperature gradients near the outer tube wall increase significantly. Close inspection of Fig. 7 shows that as the Reynolds number is increased from 350 to 1225, the effect of inner tube conduction becomes less important in the lower reaches of the tube.

3.2.2. *Effect of inner tube conductance.* The overall effect of inner tube conductance on heat transfer rate is shown in Fig. 8 using the limiting inner tube boundary conditions: zero tube conductivity (perfect insulator) and infinite tube conductivity (perfect conductor). Firstly, consider the perfectly insulated inner tube (diamonds). This is the ideal situation since no heat is then transferred back into the entering fluid. Fig. 8 reveals that the gradual spread of turbulence creates a close approximation to a simple power law relation between Nu and Re; this was also seen in Fig. 6. Onset in the inner tube has little effect on heat transfer. For the perfectly conducting inner tube (triangles), the conservative situation, the overall performance is lowered by back conduction but the curve still approxi-

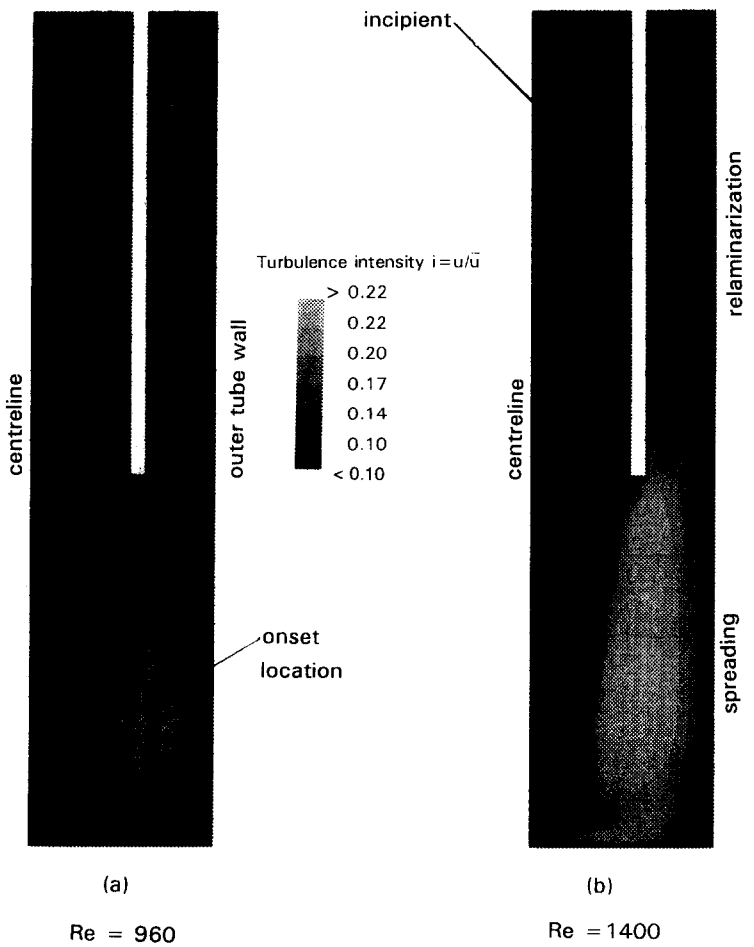

Fig. 5. The origin and spread of turbulence.

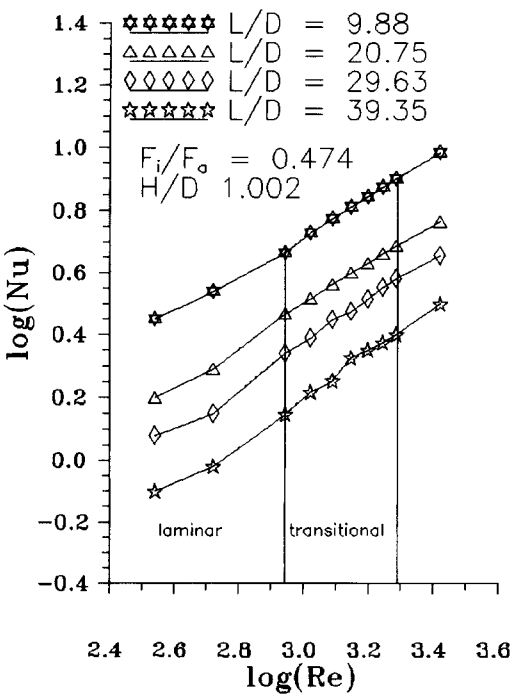

Fig. 6. Effect of Reynolds number on Nusselt number for a perfectly conducting inner tube.

mates a simple power law. The effect of back conduction was estimated by modelling the system as a set of thermal resistors in parallel (clearance and annulus zones) and series (across the annulus, inner tube and entering fluid). This yields (see Appendix)

$$Nu = \frac{Nu_{\text{cond}}}{1-c(Re)}\left[1-\frac{bc(Re)}{b+\dfrac{\lambda_f}{\lambda_i}}\right] \tag{12}$$

where $b = 0.01566$ and $c(Re)$, is the maximum fraction of heat transfer by back conduction found from the extremal values of Nu i.e. Nu_{cond} and Nu_{ins}; typically, $c \ll 1$. Using previous work in which $\lambda_f/\lambda_i = 0.01143$, this prediction is shown dashed in Fig. 8 along with comparable experimental data [14]. Agreement is well within the experimental error of $\pm 10\%$, thus suggesting that this simple model will be useful in predicting back conduction in other circumstances.

3.2.3. *Effect of length-diameter ratio.* Figure 9, which is in essence a cross plot of Fig. 6, shows the variation of Nusselt number with length–diameter ratio for several values of Reynolds number. As expected, the Nusselt number decreases with an

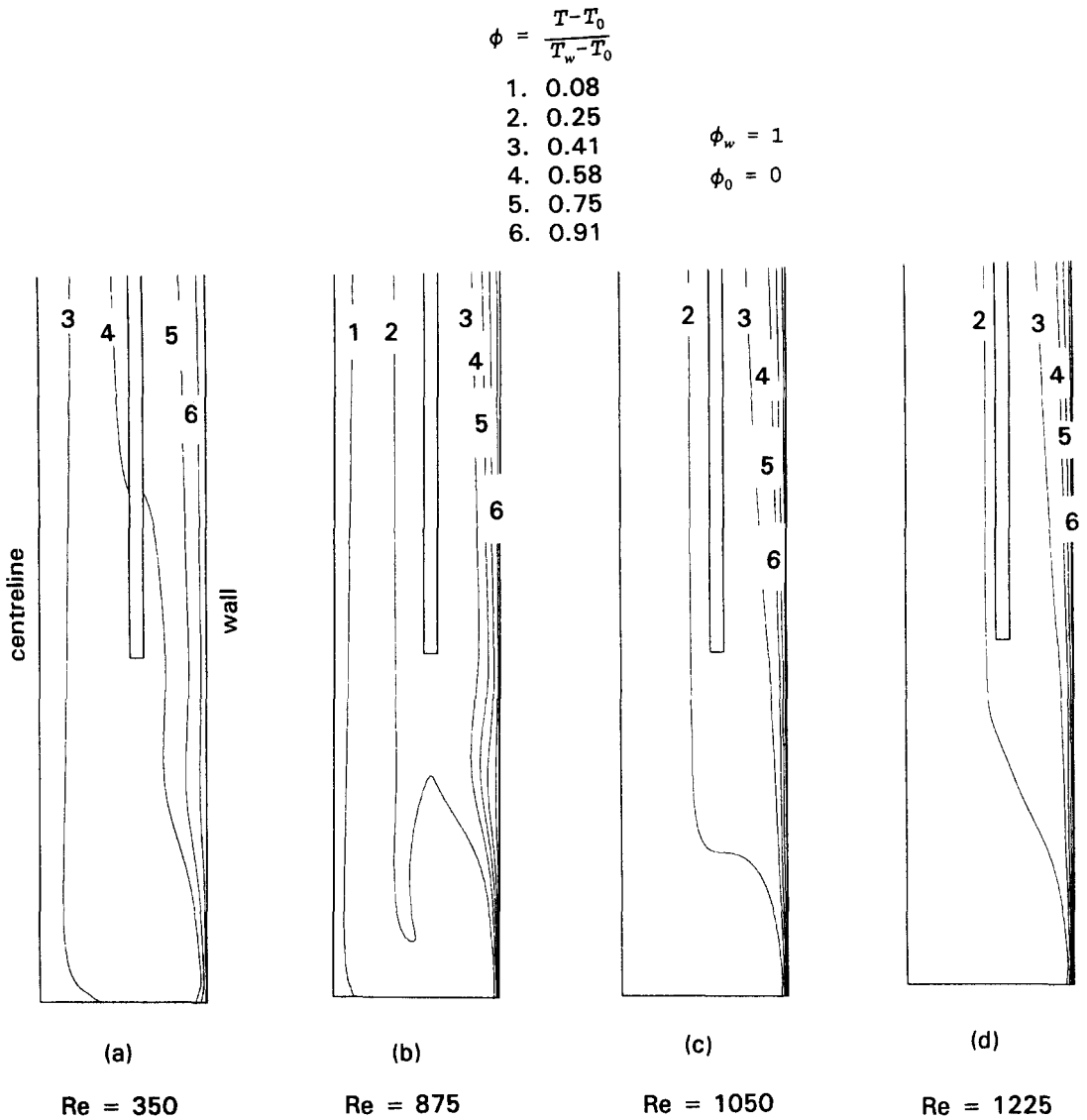

Fig. 7. Isotherms for Re = 350, 875, 1050 and 1225 with a perfectly conducting inner tube.

increase in L/D. It is interesting to note that the slope of these curves changes with L/D. For $L/D < 30$, the slope (-0.61) is less than for laminar flows [14], where Nu is inversely proportional to L/D, approximately. Examination of isotherms showed that the steepening effect at higher values of L/D may be attributed to a higher back conduction.

3.2.4. *Empirical correlation.* The selected results given above are a systematic attempt to uncover the effects of tube length, flow rate and conductance on thermal behaviour. However, while they provide a useful sensitivity study they are limited in their direct application to a wide range of industrial and geotechnical situations. For design purposes, the numerical data obtained were used to develop an empirical correlation with Nusselt number as the dependent variable. The results are shown in Fig. 10.

To construct a suitable empirical correlation form it was decided at the outset that the effect of Reynolds number could be represented by a power law, as suggested by Fig. 6. A similar assumption was made for the effect of length–diameter ratio, but Fig. 9 reveals this to be only a rough approximation. However, for design purposes a more accurate curve fit does not seem warranted. The effect of conductivity ratio was introduced through equation (12). A general relationship was thus constructed in the product form.

$$Nu = A_0(Re)^{\alpha}\left[\frac{L}{D}\right]^{\beta} f\left[c(Re), \frac{\lambda_f}{\lambda_i}\right] \tag{13}$$

where α and β are exponents, and $c(Re)$ is the maximum back conduction defined by:

$$c(Re) = 1 - \frac{Nu_{\text{cond}}}{Nu_{\text{ins}}}. \tag{14}$$

This empirical correlation yielded

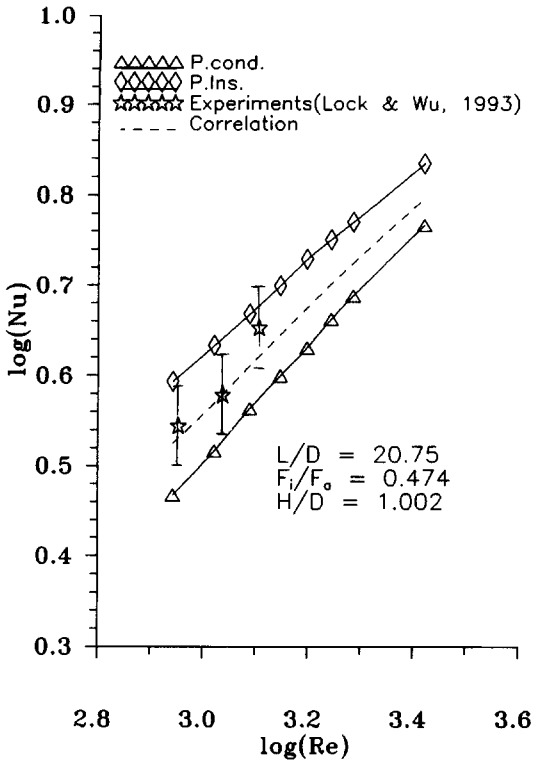

Fig. 8. Effect of the conductivity-ratio on the Nusselt number.

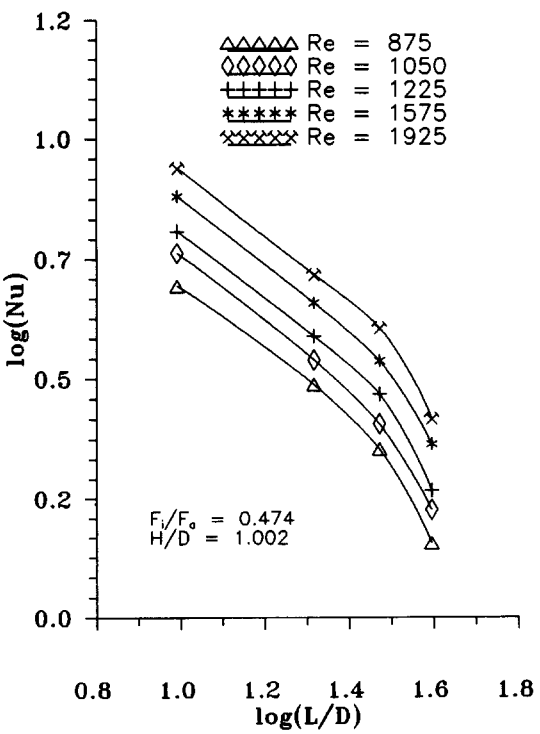

Fig. 9. Effect of the length–diameter ratio on Nusselt number for a perfectly conducting inner tube.

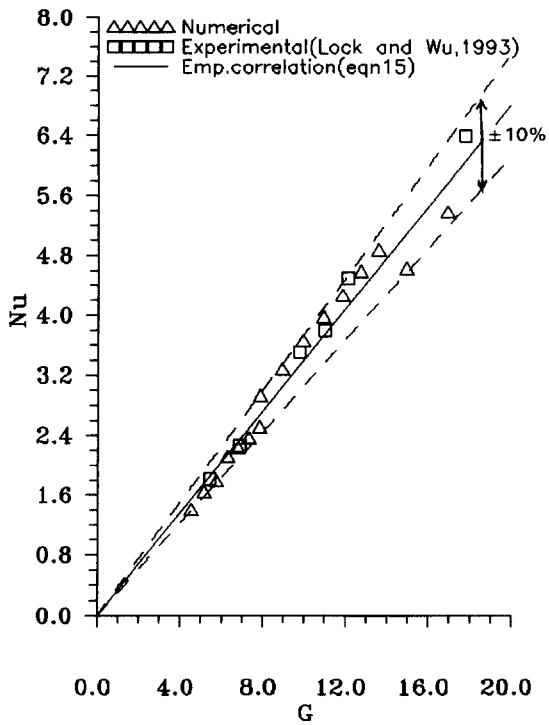

Fig. 10. The empirical correlation.

$$Nu = 0.34G \tag{15}$$

where

$$G = (Re)^{0.69}\left[\frac{L}{D}\right]^{-0.86}\frac{1}{1-c(Re)}\left[1-\frac{c(Re)}{1+\frac{\lambda_f}{\lambda_i}}\right] \tag{16}$$

and $0.14 < c < 0.26$: the mean values of α, β were found in the ranges $0.56 < \alpha < 0.91$ and $-0.78 < \beta < -1.25$.

Figure 10 shows equation (15) superimposed on transitional experimental data [14] and representative numerical data from this study. The data almost all fall within a band of $\pm 10\%$, the experimental error. This uncertainty is greater than the intrinsic numerical accuracy of $\pm 3\%$, mainly because of the approximations made in the assumed empirical form, especially the influence of L/D. It is, however, acceptable for most industrial and geotechnical applications of the bayonet tube when F_i/F_a is fixed near the 'optimal' value of 0.474 and $H/D \approx 1.0$.

Satisfactory though this correlation is, it still leaves the designer to determine T_f. To convert this to the known temperature T_0, it is only necessary to introduce the overall Nusselt number Nu_0 in which T_f is replaced by T_0 in equation (10). Recognizing that $T_f = T_f(Re, L/D, \lambda_f/\lambda_i)$, the numerical data were examined and it was found that

$$Nu_0 = 0.68\,Nu \tag{17}$$

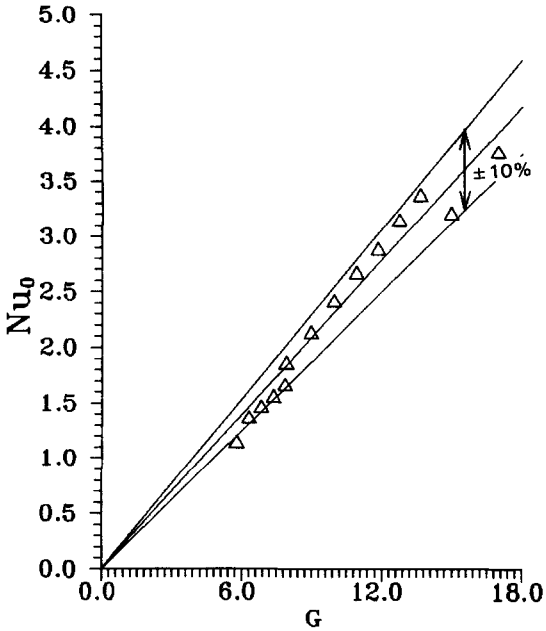

Fig. 11. The design correlation.

within ±10%. The design correlation Nu_0 vs G is presented in Fig. 11.

4. CONCLUSIONS

The paper presents numerical data for fluid flow and heat transfer in a bayonet tube during the laminar–turbulent transition. Results have been obtained for the steady flow of air in a cylindrical tube with a fixed geometry, except for the tube length. The Reynolds number and the length–diameter ratio were taken as the main independent variables, with the Nusselt number as the dependent variable. Parametric effects were examined in relation to the evolution of the turbulence intensity and temperature fields. Good agreement with previous experimental data was demonstrated.

The Nusselt number was found to increase monotonically with Reynolds number, as expected. The onset of turbulence was marked by a shallow discontinuity in the Nu–Re curve near $Re = 875$. The effect of back conduction was found to be small. The maximum variation was less than 26%. The effect was successfully described by a simple correlation. The Nusselt number decreased with L/D, as expected. An increased slope at higher L/D is attributed to a higher back conduction effect. The effects of individual parameters were each expressed in a simple design correlation. The correlation may be useful for designers concerned with thermal behaviour during the laminar-turbulent transition.

Acknowledgements—This work was made possible through the support of Natural Sciences and Engineering Research Council of Canada to whom we are indebted. We also wish to thank Mark Ackerman for assistance in the use of computational facilities in the Mechanical Engineering Department.

REFERENCES

1. Lock, G. S. H., *The Tubular Thermosyphon*. Oxford University Press, New York, 1992.
2. Jahns, H. O., Miller, T. W., Power, L. D., Rickey, W. P., Taylor, T. P. and Wheeler, J. A., Permafrost protection for pipelines on permafrost. *Second International Conference on Permafrost*. National Academy Press, Washington, DC, 1973, pp. 673–684.
3. Haynes, F. D. and Zarling, J. P., A comparative study of thermosyphons used in freezing soil. ASME paper 82-Wa/HT-40, 1982.
4. Lock, G. S. H., Control of spring runoff in northern rivers: the ice veil concept. *Polar Record*, 1986, **23**, 451–457.
5. Hurd, N. L., Mean temperature difference in field or bayonet tube, *Industrial Engineering and Chemistry*, 1946, **38**(12), 1266–1271.
6. Fraas, A. P., A potassium-steam binary vapour cycle for better fuel economy and reduced thermal pollution. *Journal of Engineering Power*, 1973, **95**, 53–63.
7. Zhang, Y. M. and Zhang, H. Q., Experimental investigation of flow characteristics about tip heat transfer in bayonet tube. *Huagong Jixie*, 1988, **15**(2), 96–102 (in Chinese).
8. Hinchley, P., Key aspects of the design and specification of individual items of plant. In *Heat Exchanger Design Handboook*, ed. B. A. Bolding and M. Prescot. Hemisphere, Washington, DC, 1984, pp. 3:16.2-1–3:16.2–15.
9. Luu, M. and Grant, K. W., Thermal and fluid design of a bayont tube heat exchanger for high temperature waste heat recovery. In *Industrial Heat Exchangers*, ed. A. J. Hayes, W. W. Wang, S. C. Richlen and E. S. Tabb. American Society for Metals, Pennsylvania, 1985, pp. 159–173.
10. Idel'chik, I. E. and Ginzburg, Y. L., The hydraulic resistance of 180° annular bends. *Teploenergetika*, 1968, **4**, 109–114.
11. Yang, S. L. and Hsieh, C. K., Fluid flow and heat transfer in a single pass, return flow, bayonet heat exchanger. *Proceedings of the ASME, AICHE, National Heat Transfer Conference*, Vol. 3, Houston, TX, pp. 355–364.
12. Lock, G. S. H. and Wu, M., Laminar frictional behaviour of a bayonet tube. *Proceedings of the Third International Symposium on Cold Regions Heat Transfer*, Fairbanks, AK, 1991, pp. 429–440.
13. Minhas, H. S., The bayonet tube: a numerical analysis of laminar frictional characteristics. M.Sc. Thesis, University of Alberta, Edmonton, Alberta, 1993.
14. Lock, G. S. H. and Wu, M., Heat transfer characteristics of bayonet tube using air under laminar conditions. *International Journal of Heat and Mass Transfer*, 1993, **36**(2), 287–291.
15. Van doormal, J. P. and Raithby, G. D., Enhancement of the SIMPLE method for predicting incompressible fluid flows. *Numerical Heat Transfer*, 1984, **7**, 147–163.
16. Jones, W. P. and Launder, B. E., The prediction of laminarization with a two-equation model of turbulence. *International Journal of Heat and Mass Transfer*, 1972, **15**, 301–314.
17. Giel, P. W. and Schmidt, W., A comparison of turbulence modelling predictions to experimental measurements for high Rayleigh number natural convection in enclosures. *Proceedings of the International Heat Transfer Conference*, Vol. 2, Jerusalem, Israel, 1990, pp. 175–180.
18. Launder, B. E. and Sharma, B. T., Application of the energy dissipation model of turbulence to the calculation of flow near a spinning disc. *Letters to Heat and Mass Transfer*, 1974, **15**, 1787.

19. Minhas, H. and Lock, G. S. H., Numerical analysis of heat transfer in an air-filled bayonet tube under laminar conditions. *International Journal of Heat and Mass Transfer*, 1995, **39**(4), 761–769.
20. Minhas, H., Lock, G. S. H. and Wu, M., Flow characteristics of an air-filled bayonet tube under laminar conditions. *International Journal of Heat & Fluid Flow*, 1995, **16**, 186–193.

APPENDIX

The effect of inner tube wall conductance

Because the heat lost by conduction from the annulus fluid is all gained by the fluid inside the inner tube, the leakage has no effect on T_f. Hence from equation (10)

$$\frac{Nu}{Nu_{ins}} = \frac{\dot{Q}}{\dot{Q}_{ins}} \tag{A1}$$

from which the leakage fraction

$$\frac{\dot{Q}_l}{\dot{Q}_{ins}} = 1 - \frac{Nu}{Nu_{ins}} \tag{A2}$$

may be assigned the maximum value c corresponding to a perfectly conducting inner tube. That is

$$\frac{(\dot{Q})_{max}}{\dot{Q}_{ins}} = 1 - \frac{Nu_{cond}}{Nu_{ins}} = c. \tag{A3}$$

Now the leakage heat transfer rate is given by

$$\dot{Q}_l = \frac{(T_f - T_0)}{R_e} \tag{A4}$$

where

$$R_e = \frac{\left(\frac{1}{h_a} + \frac{1}{h_i} + \frac{W}{\lambda_i}\right)}{A_a}$$

is the thermal resistance to leakage, and h_a, h_i are the heat transfer coefficients on either side of the inner tube wall. Letting $h = \lambda_f / B\delta$, where δ is the unknown thickness of the laminar layer adjacent to the inner tube wall, and B is an unknown constant, the thermal resistance may be rewritten

$$R_e = \frac{W}{\lambda_f A_a}\left(b + \frac{\lambda_f}{\lambda_i}\right) \tag{A5}$$

where

$$b = \frac{(B_a \delta_a + B_i \delta_i)}{W}$$

is an unknown number. This reveals that the minimum resistance to leakage occurs when

$$Re = \frac{Wb}{\lambda_f A_a}.$$

Hence, using equation (A4), the heat leakage expressed as a fraction of the maximum value is

$$\frac{\dot{Q}_l}{(\dot{Q}_l)_{max}} = \frac{b}{b + \frac{\lambda_f}{\lambda_i}}. \tag{A6}$$

This, together with equations (A2) and (A3) reveals that

$$Nu = \frac{Nu_{cond}}{1-c}\left[1 - \frac{bc}{b + \frac{\lambda_f}{\lambda_i}}\right]. \tag{A7}$$